Supplement of Atmos. Chem. Phys., 18, 5549–5565, 2018
https://doi.org/10.5194/acp-18-5549-2018-supplement

Atmospheric Chemistry and Physics
Open Access
EGU

Supplement of

Novel pathway of SO_2 oxidation in the atmosphere: reactions with monoterpene ozonolysis intermediates and secondary organic aerosol

Jianhuai Ye et al.

Correspondence to: Arthur W. H. Chan (arthurwh.chan@utoronto.ca)

S1. Synergistic effect between SOA formation and SO_2 oxidation under ozone-limited conditions

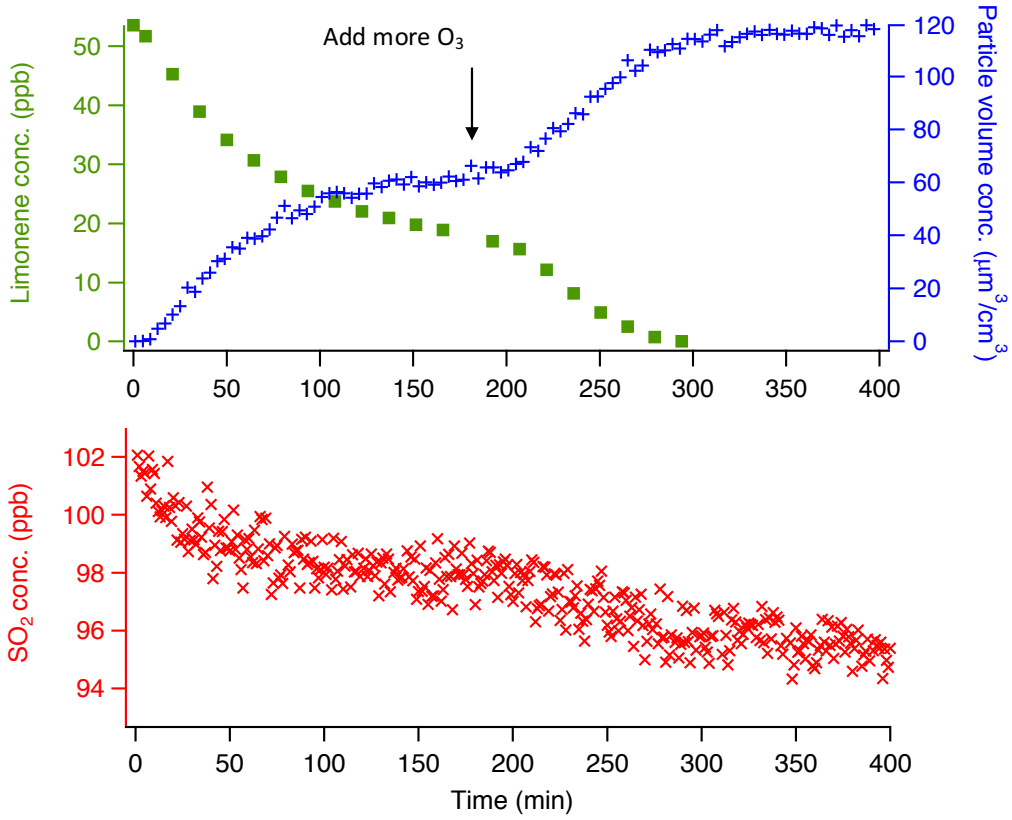

Figure S1 Particle volume concentration, limonene concentration and SO_2 concentration as a function of experimental time with stepwise ozone injection. Ozone was injected into the chamber that was prefilled with limonene until it reached around 50 ppb (the same as initial limonene concentration). Additional ozone was added at 180 min.

S2. SO_2 consumption in the presence of formic acid under dry or humid conditions

A. No formic acid under dry condition

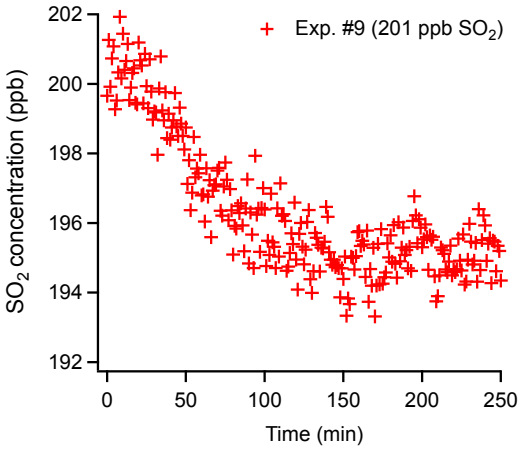

B. With formic acid under dry condition

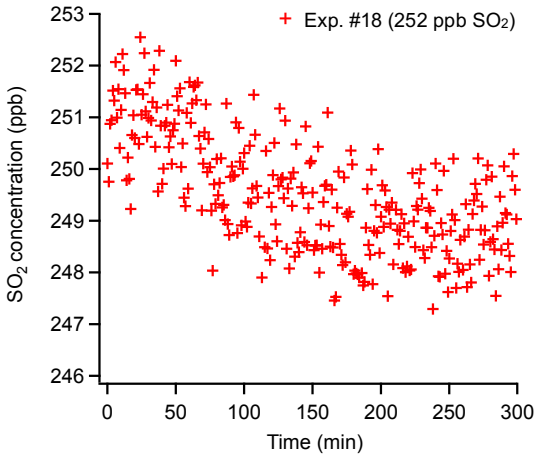

C. With formic acid under humid condition

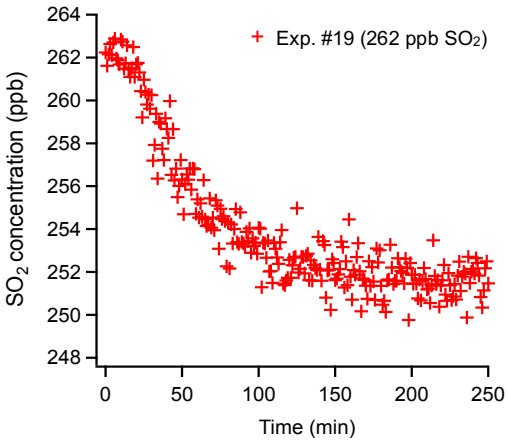

Figure S2 SO_2 consumption over the course of the experiments for Exp. #9 (panel A, no formic acid under dry condition), Exp. #18 (panel B, with formic acid under dry condition) and Exp. #19 (panel C, with formic acid under humid condition). By adding formic acid into SOA reaction, less SO_2 consumption was observed under dry conditions (Exp. #18 vs Exp. #9). However, under humid conditions, significant SO_2 depletion was detected even with sufficient addition of formic acid as Criegee intermediate scavenger (Exp. #19 vs Exp. #9).

S3. Interactions between SO_2 and peroxides

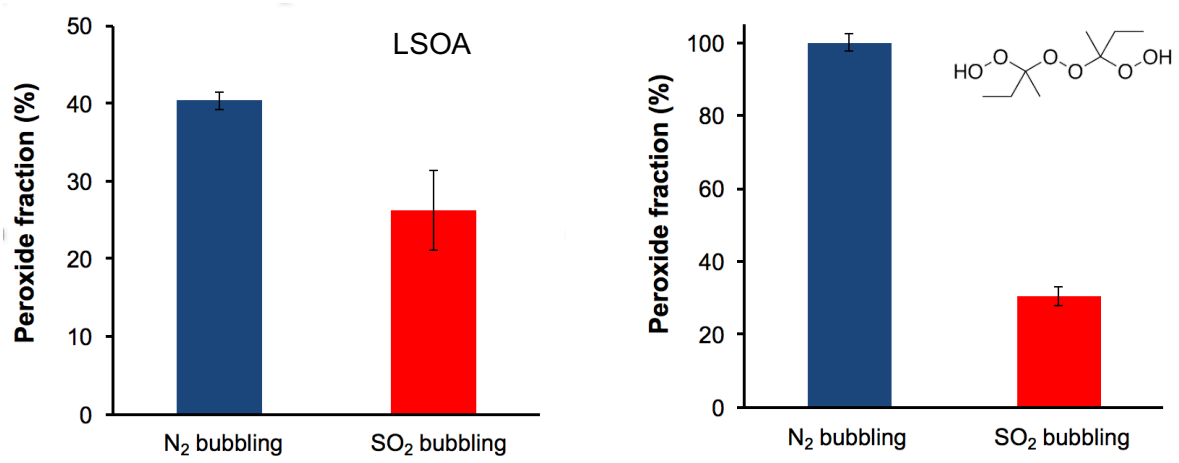

Figure S3 Peroxide fractions in SOA solution bubbled with N_2 and SO_2. Lower peroxide fraction was detected when bubbling SO_2 into LSOA solution (left panel). Significant decrease in peroxide content was also observed when bubbling SO_2 into 2-butanone peroxide solution (right panel), highlighting the importance of organic peroxide in SO_2 oxidation.

S4. SO_2 reactions with other oxidants and SO_3 experiment

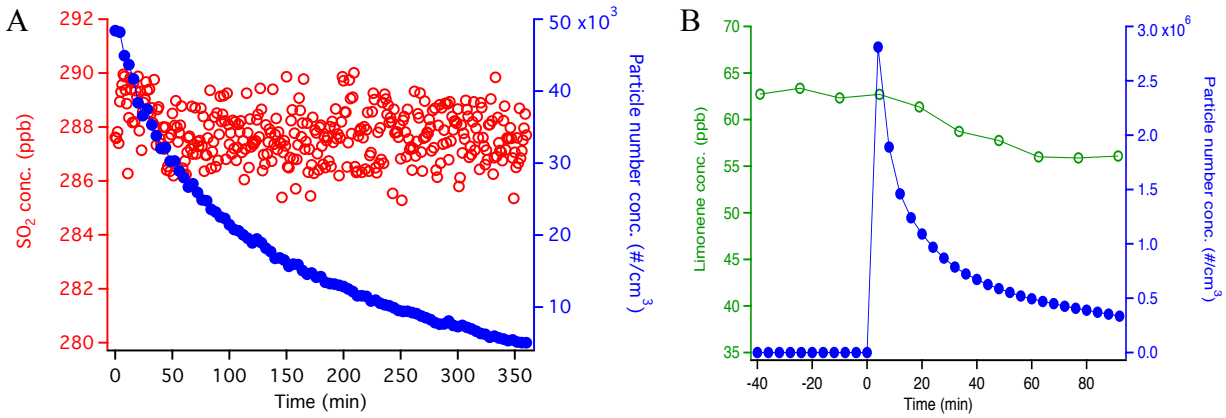

Figure S4 Two sets of control experiments to investigate other potential oxidants of SO_2. Panel A shows the change in SO_2 and particle (ammonium sulfate) concentration as a function of time in the presence of ozone (485 ppb) and formic acid (13 ppm) under humid condition (50% RH). Panel B shows the change in limonene and particle (sulfuric acid) concentration as a function of time. It is noted that in both figures, particle concentration was not corrected for chamber wall loss.

S5. Identification of organosulfates

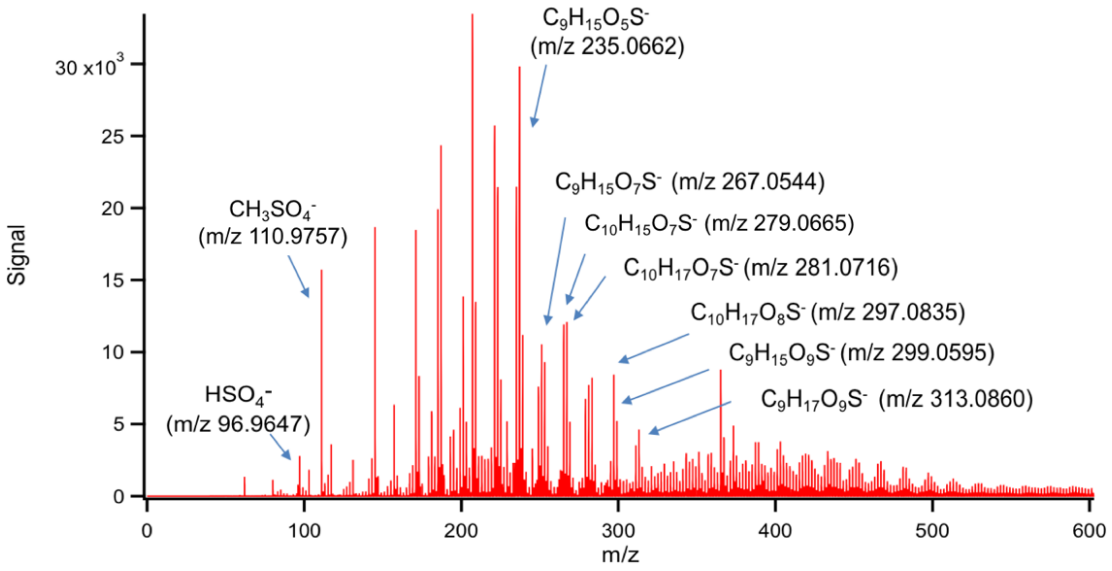

Figure S5 Organosulfates observed using IMS-TOF

Table S1 Identification of sulfur-containing ions based on IMS drift time and Kendrick mass defect

1) SO_2 : Limonene = 100 ppb : 500 ppb

Entry	$[M - H]^-$	Proposed formula for $[M - H]^-$	MW (M)	Identification Methods
1	96.9647	HSO_4^-	98	Mass calibration
2	110.9757	$CH_3SO_4^-$	112	IMS drift time with HSO_4^-
3	235.0662	$C_9H_{15}O_5S^-$	236	Kendrick mass defect (O) with $C_9H_{15}O_9S^-$ Kendrick mass defect (CO_2) with $C_{10}H_{15}O_7S^-$
4	267.0544	$C_9H_{15}O_7S^-$	268	Kendrick mass defect (C) with $C_{10}H_{15}O_7S^-$ Kendrick mass defect (CH_2) with $C_{10}H_{17}O_7S^-$
5	279.0665	$C_{10}H_{15}O_7S^-$	280	IMS drift time with $CH_3SO_4^-$
6	281.0716	$C_{10}H_{17}O_7S^-$	282	IMS drift time with $CH_3SO_4^-$
7	297.0835	$C_{10}H_{17}O_8S^-$	298	IMS drift time with $CH_3SO_4^-$
8	299.0595	$C_9H_{15}O_9S^-$	300	Kendrick mass defect (CH_2O) with $C_{10}H_{17}O_8S^-$ Kendrick mass defect (CH_2) with $C_{10}H_{17}O_9S^-$
9	313.0860	$C_{10}H_{17}O_9S^-$	314	IMS drift time with $CH_3SO_4^-$

2) SO_2 : Limonene = 250 ppb : 500 ppb

Entry	$[M - H]^-$	Proposed formula for $[M - H]^-$	MW (M)	Identification Methods
1	79.9573	SO_3^-	n/a	IMS drift time with HSO_4^-
2	96.9631	HSO_4^-	98	Mass calibration
3	110.9758	$CH_3SO_4^-$	112	IMS drift time with HSO_4^-
4	124.9914	$C_2H_5SO_4^-$	126	Kendrick mass defect (CH_2) with HSO_4^-, $CH_3SO_4^-$
5	179.0383	$C_6H_{11}O_4S^-$	180	Kendrick mass defect (O) with $C_6H_{11}O_8S^-$
6	186.9554	$C_2H_3O_8S^-$	188	IMS drift time with HSO_4^-
7	194.9275	$HSO_4^-(H_2SO_4)$	196	IMS drift time with HSO_4^-
8	200.9711	$C_3H_5O_8S^-$	202	IMS drift time with HSO_4^-
9	211.0282	$C_6H_{11}O_6S^-$	212	Kendrick mass defect (O) with $C_6H_{11}O_8S^-$
10	223.0282	$C_7H_{11}O_6S^-$	224	Kendrick mass defect (CH_2O) with $C_9H_{15}O_7S^-$ Kendrick mass defect (C) with $C_{12}H_{11}O_6S^-$
11	225.0438	$C_7H_{13}O_6S^-$	226	Kendrick mass defect (CH_2) with $C_6H_{11}O_6S^-$
12	229.0024	$C_5H_9O_8S^-$	230	Kendrick mass defect (CH_2) with $C_3H_5O_8S^-$
13	235.0645	$C_9H_{15}O_5S^-$	236	Kendrick mass defect (CO_2) with $C_{10}H_{15}O_7S^-$
14	239.0231	$C_7H_{11}O_7S^-$	240	Kendrick mass defect (O) with $C_9H_{15}O_7S^-$
15	243.0180	$C_6H_{11}O_8S^-$	244	IMS drift time with HSO_4^-
16	267.0544	$C_9H_{15}O_7S^-$	268	IMS drift time with HSO_4^-
17	279.0544	$C_{10}H_{15}O_7S^-$	280	IMS drift time with HSO_4^-
18	283.0307	$C_{12}H_{11}O_6S^-$	283	IMS drift time with HSO_4^-
19	299.0442	$C_9H_{15}O_9S^-$	300	Kendrick mass defect (O) with $C_9H_{15}O_7S^-$

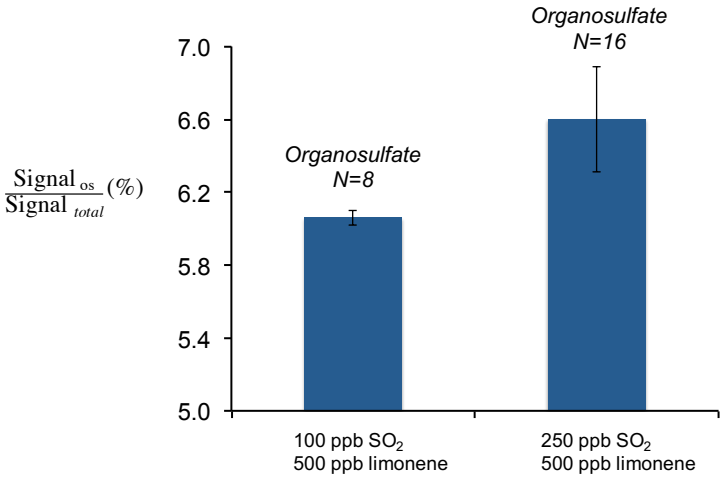

Figure S6 Fraction of total organosulfates with different SO_2 injection concentration in SOA formation. Both the amount and the types of organosulfates increase with increasing SO_2 concentration.

S6. Effect of SO_2 on α-pinene SOA formation

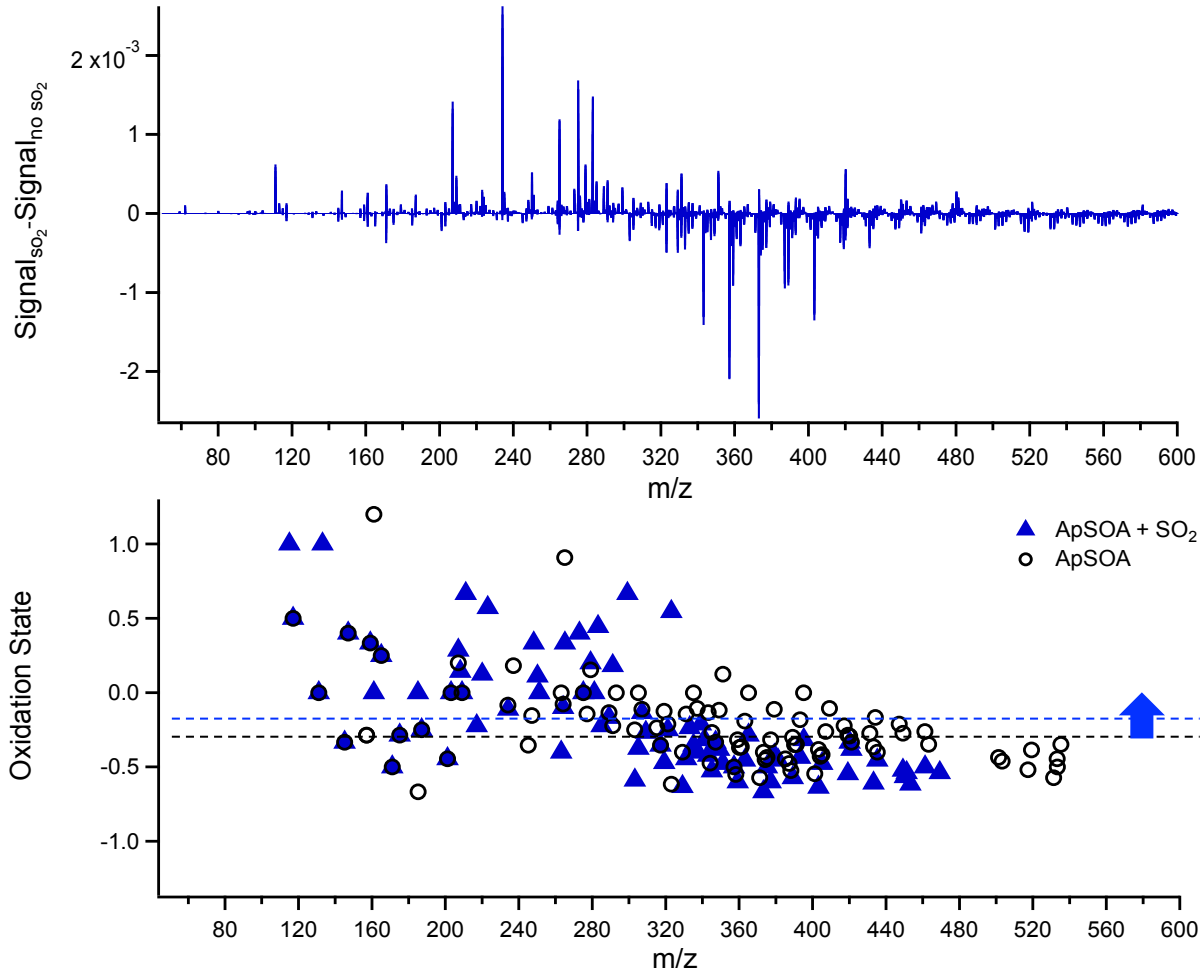

Figure S7 Difference in normalized mass spectra between α-pinene SOA (ApSOA) formed in the presence and absence of SO_2 (top panel). Signal of HSO_4^- (m/z 96.96) was not included in figure to investigate changes in the organic mass only. Bottom panel shows the average carbon oxidation state of each peak detected in IMS-TOF and the overall average oxidation states of ApSOA (black dashed line) and ApSOA + SO_2 (blue dashed line).

S7. Gas-phase kinetic model for SO_2 oxidation

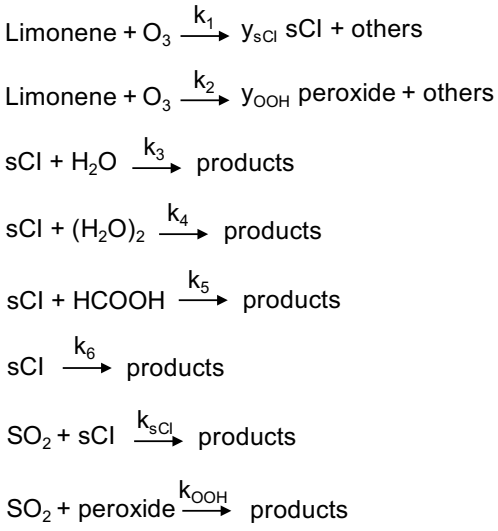

Scheme S1 Gas-phase reactions for SO_2 oxidation by sCIs and peroxides.

Shown in Scheme S1, Criegee intermediates (sCIs) and peroxides are formed from limonene ozonolysis and then react with SO_2.

For sCIs:

It is noted that different sCI conformers can be formed in monoterpene ozonolysis (Scheme 1 and Scheme S2). The information regarding the reactivities of different monoterpene sCI conformers is lacking in the literature. Therefore, reaction rate constants in Scheme 1 were estimated and shown in Table S2. Two different values of $k_{\mathrm{sCI}+SO_2}$ were used in the simulation to examine the sensitivity of different sCI + SO_2 reaction rates on SO_2 oxidation.

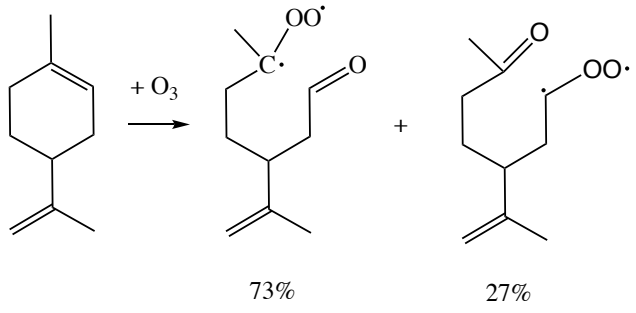

Scheme S2 Different conformers of sCIs formed from limonene ozonolysis

Table S2 Rate constants for reactions in Scheme S1

	Rate constant	Value	Note	Literature
k_1=k_2	$k_{\mathrm{lim}+O_3}$	2.1×10^{-16} cm^3 molecule^{-1} s^{-1}		(Atkinson and Arey, 2003)
k_3	$k_{\mathrm{sCI}+H_2O}$ (mono-substituted)	$8.8 \times 10^{-5}\ k_{\mathrm{sCI}+SO_2}$	Estimated from k_{sCI+H_2O} of trans-2-butene	(Berndt et al., 2014)
	$k_{\mathrm{sCI}+H_2O}$ (di-substituted)	$4.0 \times 10^{-6}\ k_{\mathrm{sCI}+SO_2}$	Estimated from $k_{\mathrm{sCI}+H_2O}$ of tetramethylethylene	(Berndt et al., 2014)
k_4	$k_{\mathrm{sCI}+(H_2O)_2}$	$1\times 10^3\ k_{\mathrm{sCI}+H_2O}$		(Huang et al., 2015)
k_5	$k_{\mathrm{sCI}+formic\ acid}$	$3 \times\ k_{\mathrm{sCI}+SO_2}$		(Sipilä et al., 2014)
k_6	$k_{decompose}$ (mono-substituted)	$1.2 \times\ 10^{12}\ k_{\mathrm{sCI}+SO_2}$ molecule cm^{-3}	Estimated from $k_{decompose}$ of trans-2-butene	(Berndt et al., 2014)
	$k_{decompose}$ (di-substituted)	$4.2 \times\ 10^{12}\ k_{\mathrm{sCI}+SO_2}$ molecule cm^{-3}	Estimated from $k_{decompose}$ of tetramethylethylene	(Berndt et al., 2014)
k_{sCI}	$k_{\mathrm{sCI}+SO_2}$ (high)	3.9×10^{-11} cm^3 molecule^{-1} s^{-1}	Estimated from $k_{\mathrm{sCI}+SO_2}$ of CH_2OO	(Welz et al., 2012)
	$k_{\mathrm{sCI}+SO_2}$(low)	8×10^{-13} cm^3 molecule^{-1} s^{-1}	Estimated by Mauldin et al. based on field observations	(Mauldin III et al., 2012)

For peroxides:

A simplified bimolecular reaction was assumed in this study. The reaction is modelled as an irreversible pathway to match the observed SO_2 decay in our experiments. The simplified model is used to qualitatively demonstrate the importance of peroxide reaction pathway under our experimental conditions. It should be noted that more information regarding the reaction mechanisms, such as the Henry's law constants of organic peroxides, is needed to accurately simulate this process.

The reaction rate between SO_2 and peroxide can be calculated as:

$$R_{SO_2+peroxide} = k_{OOH}[peroxide]\ [SO_2]$$

where k_{OOH} is the pseudo reaction rate constant (in cm^3 molecule^{-1} s^{-1}); $[peroxide]$ and $[SO_2]$ are the concentrations of peroxide and SO_2 (in molecule cm^{-3}), respectively.

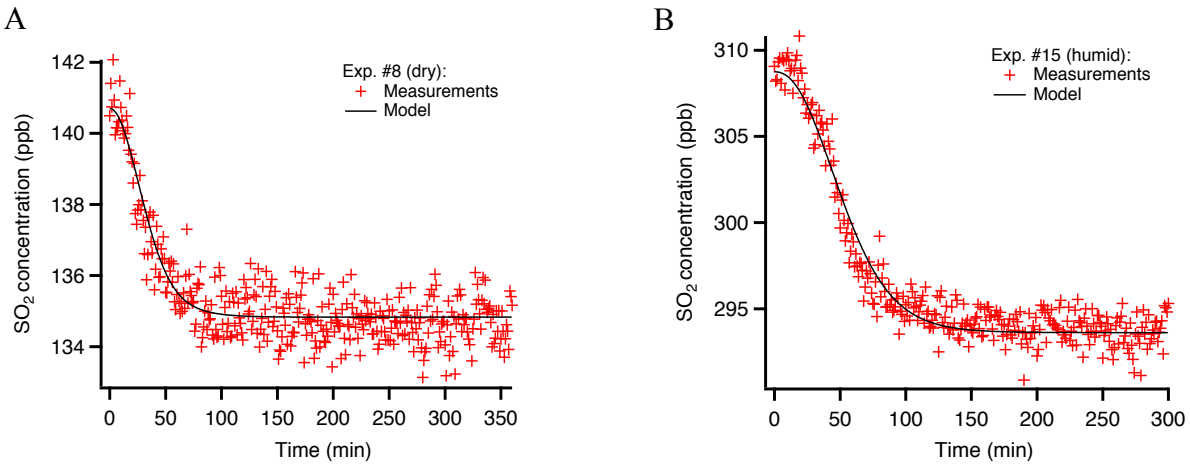

Figure S8 Examples of measured and model-simulated SO_2 concentrations under dry (A) and humid conditions (B).

Shown in Fig. S8, the time trends of SO_2 in the model simulation (Scheme S1) matches those over the course of the experiments under both dry and humid conditions. Constrained from our laboratory observations, sCI yield from limonene ozonolysis (y_{sCI}) was calculated to be 0.32, which is consistent with the results from Sipilä et al. (0.27 ± 0.12) (2014). y_{OOH} that represents the amount of peroxides in the aqueous phase that can react with SO_2, was calculated to be 0.06 and 0.43 under dry (10% RH) and humid (50% RH) conditions, respectively. This is likely because that under humid conditions, more aerosol water is available for peroxides to partition into the aqueous phase and react with SO_2. It was also observed that $k_{\mathrm{sCI}+SO_2}$ did not play an important role in SO_2 oxidation in this simulation. Little change was observed when different reaction rates ($k_{\mathrm{sCI}+SO_2}$) were used, indicating that the consumption of SO_2 was limited by the concentrations of sCIs that were available for SO_2 reaction.

S8. SO_2 uptake coefficient by reacting with peroxides

The uptake coefficient of SO_2 (γ) to the particles can be estimated using the following equation (Seinfeld and Pandis, 2006):

$$\frac{d[SO_2]}{dt} = -\frac{1}{4}\gamma A\tilde{v}\,[SO_2] \quad \text{(S1)}$$

where $[SO_2]$ is gas-phase SO_2 concentration (molecules cm^{-3}); A is the total surface area concentration of particles ($m^2\,m^{-3}$) derived from particle size distribution measured by SMPS; $\tilde{v}$ is the mean molecular speed of SO_2 ($m\,s^{-1}$) which can be calculated from:

$$\tilde{v} = \sqrt{\frac{8RT}{MW\pi}} \quad \text{(S2)}$$

where R is the gas constant; T is temperature; MW is the molecular weight of SO_2.

To calculate the uptake coefficient by peroxides, we assume that the fraction of SO_2 that reacted with peroxides ($f_{(SO_2+peroxide)}$) was constant over the course of the experiment. Eqn. (S1) can be then modified as:

$$ln\frac{[SO_2]_0}{[SO_2]_t} = \ln\frac{[SO_2]_0}{[SO_2]_0 - ([SO_2]_0 - [SO_2]_t)f_{(SO_2+peroxide)}} = \frac{1}{4}\gamma A\tilde{v}\,\Delta t \quad \text{(S3)}$$

where $[SO_2]_0$ and $[SO_2]_t$ are SO_2 concentration at 0 min and t min, respectively. Since SO_2 consumption ceased when t is around 150 min for all the limonene experiments under humid conditions, Δt = 150 min was used in all the calculations. We therefore present a conservative estimate of SO_2 uptake coefficients, shown in Table S3.

Table S3 Estimated uptake coefficients of SO_2 through reacting with peroxides from limonene ozonolysis under humid conditions

Exp. #	$[SO_2]_{0\,min}$ (ppb)	$[SO_2]_{150\,min}$ (ppb)	S ($m^2\ m^{-3}$) [a]	$f_{(SO_2+peroxide)}$ [b]	RH (%)	γ
14	144.3	128.9	2.24×10^{-3}	0.84	55%	5.1×10^{-5}
15	308.8	293.8	2.32×10^{-3}	0.76	47%	1.8×10^{-5}
19	262.2	252.2	1.73×10^{-3}	0.77	50%	1.9×10^{-5}
20	605.4	593.0	1.57×10^{-3}	0.75	52%	1.1×10^{-5}

[a]: average total particle surface area concentration in the first 150 min of the experiments;
[b]: the fraction of SO_2 that reacted with peroxides, calculated using the modeling simulation results from Section S6

Reference

Atkinson, R. and Arey, J.: Atmospheric degradation of volatile organic compounds, Chem. Rev., 103(12), 4605–4638, doi:10.1021/cr0206420, 2003.

Berndt, T., Jokinen, T., Sipilä, M., Mauldin, R. L., Herrmann, H., Stratmann, F., Junninen, H. and Kulmala, M.: H_2SO_4 formation from the gas-phase reaction of stabilized Criegee Intermediates with SO_2: Influence of water vapour content and temperature, Atmos. Environ., 89, 603–612, doi:10.1016/j.atmosenv.2014.02.062, 2014.

Huang, H.-L., Chao, W. and Lin, J. J.-M.: Kinetics of a Criegee intermediate that would survive high humidity and may oxidize atmospheric SO_2, Proc. Natl. Acad. Sci., 112(35), 10857–10862, doi:10.1073/pnas.1513149112, 2015.

Mauldin III, R. L., Berndt, T., Sipilä, M., Paasonen, P., Petäjä, T., Kim, S., Kurtén, T., Stratmann, F., Kerminen, V.-M. and Kulmala, M.: A new atmospherically relevant oxidant of sulphur dioxide, Nature, 488(7410), 193–196, doi:10.1038/nature11278, 2012.

Seinfeld, J. H. and Pandis, S. N.: Atmospheric chemistry and physics: From air pollution to climate change, 2nd Ed., Wiley: New York., 2006.

Sipilä, M., Jokinen, T., Berndt, T., Richters, S., Makkonen, R., Donahue, N. M., Mauldin III, R. L., Kurtén, T., Paasonen, P., Sarnela, N., Ehn, M., Junninen, H., Rissanen, M. P., Thornton, J., Stratmann, F., Herrmann, H., Worsnop, D. R., Kulmala, M., Kerminen, V.-M. and Petäjä, T.: Reactivity of stabilized Criegee intermediates (sCIs) from isoprene and monoterpene ozonolysis toward SO_2 and organic acids, Atmos. Chem. Phys., 14(22), 12143–12153, doi:10.5194/acp-14-12143-2014, 2014.

Welz, O., Savee, J. D., Osborn, D. L., Vasu, S. S., Percival, C. J., Shallcross, D. E. and Taatjes, C. A.: Direct kinetic measurements of Criegee intermediate (CH_2OO) formed by reaction of CH_2I with O_2, Science, 335(6065), 204–207, doi:10.1126/science.1213229, 2012.